J Appl Electrochem (2014) 44:301–307
DOI 10.1007/s10800-013-0629-z

RESEARCH ARTICLE

Isotropic magnetization response of electrodeposited nanocrystalline Ni–W alloy nanowire arrays

Takeshi Ohgai · Takafumi Fujimaru · Yoshitomo Tanaka

Received: 30 June 2013 / Accepted: 16 September 2013 / Published online: 25 September 2013

Abstract Isotropic magnetization response was demonstrated in electrodeposited nanocrystalline Ni–15 % W alloy nanowire arrays, which can be applied to nanoscale magnetic field sensors. The Ni–W alloy nanowire arrays were electrochemically synthesized on a nanochannel template electrode from an aqueous electrolytic solution. X-ray and electron diffraction patterns revealed that Ni–15 % W alloy deposits were composed of ultrafine crystal grains with a supersaturated solid solution phase. The magnetization of the Ni–15 % W alloy thin films reached saturation at around 2.5 kOe in a perpendicular direction to the film plane, whereas the pure Ni thin films hardly magnetized in the perpendicular direction. On the contrary, Ni–15 % W alloy nanowire arrays were easily magnetized, and reach saturation at around 1.0 kOe, even in a perpendicular direction to the array film plane that corresponds to the long-axis direction of the alloy nanowires.

Keywords Nanocrystalline · Nanowire · Nickel · Tungsten · Electrodeposition · Magnetization

T. Ohgai (✉)
Department of Materials Science and Engineering, Nagasaki University, 1-14, Bunkyo-machi, Nagasaki 852-8521, Japan
e-mail: ohgai@nagasaki-u.ac.jp

T. Fujimaru
Hiroshima Machinery Works, Mitsubishi Heavy Industries Ltd., 4-6-22, Kan-on-shin-machi, Nishi-ku, Hiroshima 733-8553, Japan

Y. Tanaka
Technical Center, TDK Corporation, 2-15-7 Higashi-Ohwada, Ichikawa-shi, Chiba 272-8558, Japan

1 Introduction

Tungsten (W) has the highest melting point (3,695 K) among all metals in their pure forms, so its alloys exhibit excellent mechanical strength and thermal resistance. Usually, W alloys are produced by a powder metallurgy process at high temperatures. However, Ni–W [1], Fe–W [2], and Ni–Fe–W [3] alloy thin films can be prepared by an electrodeposition process at room temperature. WO_4^{2-} ions cannot be reduced to their metallic state in aqueous solutions containing only WO_4^{2-} ions, but they can be reduced when the aqueous solutions include iron-group metal (M^{iron}) ions, such as Ni^{2+}, Co^{2+}, and Fe^{2+}. Brenner classified this reduction process into the "induced co-deposition mechanism" [4].

Electrodeposited M^{iron} alloy thin films, which contain several tens of a percentage of W, usually consist of a supersaturated solid solution phase with nano-sized crystal grains [5]. Recently, nanocrystalline metallic materials and nanoparticles have received much attention due to their unique physical properties, such as mechanical strength [6], corrosion resistance [7, 8], electron transport [9], and magnetic property [10, 11]. Nanocrystalline M^{iron}–W alloy thin films are of special value to developers, because they exhibit excellent magnetization response and corrosion resistance [12]. Hence, M^{iron}–W alloy thin films can be applied to magnetic field sensors that are used for monitoring magnetic fields in corrosive environments, such as monitoring the wheel rotation rate in an automobile's antilock brake system [13]. These magnetic field sensors will be required to sense the field three-dimensionally. However, the conventional magnetic thin film sensors are hardly magnetized in a perpendicular direction to the film plane due to the large demagnetizing field caused by the inverse magnetic poles generated on the film surfaces [14].

On the other hand, nanoparticle-integrated structures [15, 16] with strong shape magnetic anisotropy, such as electrodeposited M^{iron} magnetic nanowire arrays [17–19], can be magnetized even in a direction that is perpendicular to the array film plane, but the coercive force reaches around several hundreds of Oersted, which is too large to be applied to a conventional magnetic field sensor. To improve the soft magnetic property of the M^{iron} nanowire array, the magnetocrystalline anisotropy (K_C) should be decreased. If nanocrystalline M^{iron}–W alloy nanowire arrays are synthesized by the electrodeposition technique, then a three-dimensional nanoscale magnetic field sensor will be realized.

In this study, the nanocrystalline structure and magnetization behavior of Ni–W alloy nanowire arrays were synthesized from acidic aqueous solutions by using an induced co-deposition technique to develop a corrosion-resistant nanoscale magnetic field sensor with an isotropic magnetization response.

2 Experiment

The bath compositions for the electrodeposition of the Ni–W alloys are shown in Table 1. The electrolytic solutions were synthesized from the following chemicals: $NiSO_4{\cdot}6H_2O$, $Na_2WO_4{\cdot}2H_2O$, $FeSO_4{\cdot}7H_2O$, and $C_3H_4(OH)(COOH)_3$ (citric acid). The solution's pH was adjusted to 2.0 by adding H_2SO_4 and NaOH. An ion track-etched polycarbonate membrane filter with numerous nanochannels (pore diameters of 80 and 160 nm, pore length of 6 μm, and pore density of 6×10^8 pores·cm^{-2}) was used as a template for growing Ni–W alloy nanowires, while a copper foil was used as a cathode for the electrodeposition of the Ni–W alloy thin films. On the surface of the membrane filter, a gold layer was sputter-deposited to cover the pores and to create a cathode. A gold wire and a Ag/AgCl electrode were used as the anode and reference electrode, respectively. To determine the optimum cathode potential for the electrodeposition of Ni–W alloys, a cathode polarization curve was plotted over the wide potential range from 0 to −2.0 V. According to the cathode polarization curve, the cathode current density (CCD) increased at around −0.7 V due to the beginning of the Ni–W alloys' electrodeposition. In the potential region of less than −2.0 V, the cathode's potential polarized significantly to a less-noble region as the CCD increased. This polarization was caused by the diffusion limit of Ni^{2+} and WO_4^{2-} ions. The surface appearance of the metal electrodeposits changed from an ideal smooth surface to powder-like rough deposits as the CCD increased to the diffusion limit of the metal ions. Therefore, the optimum cathode potential for the electrodeposition of Ni–W alloys was determined to be −1.5 V versus Ag/AgCl at 313 K.

Table 1 Bath compositions for the electrodeposition of Ni–W alloys

Electrolyte (mol/L)			WO_4^{2-} concentration ratio in baths (%)
$[WO_4^{2-}]$	$[Ni^{2+}]$	$[C_6H_5O_7^{3-}]$	R_W^{bath}
0	0.5	0.5	0
0.025	0.475	0.5	5
0.05	0.45	0.5	10
0.1	0.4	0.5	20
0.15	0.35	0.5	30
0.2	0.3	0.5	40
0.25	0.25	0.5	50

After growing the Ni–W alloy nanowire arrays, polycarbonate nanochannel templates were dissolved in an organic solvent and the remains, which consisted of electrodeposited Ni–W alloy nanowires, served as the samples for the SEM and TEM observations. To investigate the relationship between the WO_4^{2-} concentration ratio in the solutions ($R_W^{bath} = 100 \times [WO_4^{2-}]/([WO_4^{2-}] + [Ni^{2+}])$) and the W content in the deposits ($R_W^{depo} = 100 \times [W]/([W] + [Ni])$), the chemical composition of the alloy deposits was determined using energy dispersive X-ray spectrometry. The constituent phase and crystallinity of the electrodeposited Ni–W alloy thin films and nanowire arrays were defined by X-ray diffraction and electron beam diffraction. The magnetization behavior of the alloy thin films and nanowire arrays was investigated by a vibrating sample magnetometer (VSM) with an increasing magnetic field up to 10 kOe. The magnetic field was applied in-plane or in perpendicular directions to the surface of the substrates.

3 Results and discussion

3.1 Structure of the electrodeposited Ni–W alloy nanowires

Figure 1 shows the relationship between the WO_4^{2-} concentration ratio (R_W^{bath}) and the W content in the alloy deposits (R_W^{depo}). If R_W^{depo} equals R_W^{bath} ($R_W^{depo} = R_W^{bath}$), then the plotted points are on the composition reference line (CRL). As shown in Fig. 1, R_W^{depo} increased with an increase in R_W^{bath}. At each plotted point, R_W^{depo} is smaller than R_W^{bath}, which indicates that Ni preferentially electrodeposits, whereas W does not. For example, a Ni–15 at.% W alloy ($R_W^{depo} = 15$ %) was obtained from a solution containing 40 % WO_4^{2-} ions as a molar concentration ratio ($R_W^{bath} = 40$ %). In this condition, R_W^{depo} was diluted ca. 0.4 times lower than R_W^{bath}. WO_4^{2-} ions cannot reduce to a metallic state in an aqueous solution that

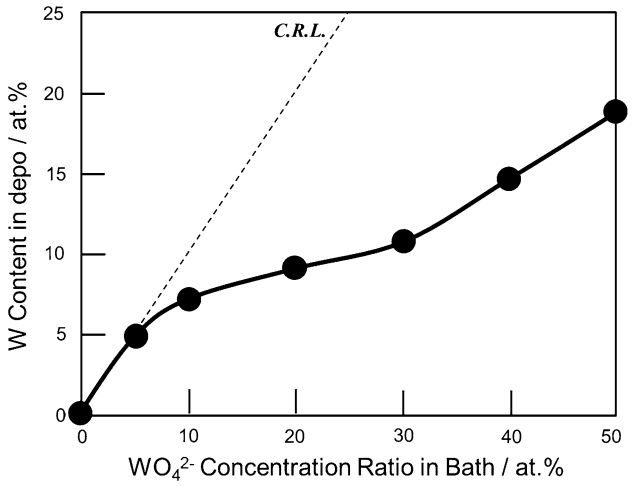

Fig. 1 Relationship between WO_4^{2-} concentration ratio in baths (R_W^{bath}) and W content in Ni–W alloy deposits (R_W^{depo})

contains only WO_4^{2-} ions. However, they can reduce to a metallic state as an alloy in an aqueous solution containing WO_4^{2-} ions in the presence of iron-group metal ions, such as Ni^{2+}, Co^{2+}, and Fe^{2+}. This reduction process is known as the "induced co-deposition mechanism," and the co-deposition behavior, which appears in Fig. 1, can be explained with this mechanism. Metzler et al. [20] have estimated that citrate ions will exist as H_2Cit^- in a solution with a pH 2 and that WO_4^{2-} will exist as $[(WO_4)(Cit)H_2]^{3-}$ complex ions at a pH 2. In this study, as shown in Fig. 1, R_W^{depo} was diluted ca. 0.4 times lower than R_W^{bath}. This dilution of W in the alloy deposits results from the existence of stable $[(WO_4)(Cit)H_2]^{3-}$ complex ions. Admon et al. [21] reported on the electrodeposition process of ferromagnetic Co–W alloys, revealing that R_W^{depo} increases with an increase in R_W^{bath} and that Co preferentially electrodeposits rather than W. For their study, they obtained a Co–32 at.% W alloy ($R_W^{depo} = 32$ %) from a solution containing 46 % WO_4^{2-} ions as a molar concentration ratio ($R_W^{bath} = 46$ %). Hence, they diluted R_W^{depo} ca. 0.7 times lower than R_W^{bath}. According to the "induced co-deposition mechanism," the reduction ability of iron-group metals depends on the number of unpaired electrons [22]. The number of unpaired 3d electrons of Ni, Co, and Fe are 0.6, 1.6, and 2.2, respectively, so the reduction ability of Ni is only 0.375 times than that of Co. Therefore, in this study, the dilution of WO_4^{2-} in the alloy deposits from the solution containing Ni^{2+} ions should have been caused by the small reduction ability of electrodeposited Ni.

Figure 2 shows the X-ray diffraction profiles obtained from electrodeposited pure Ni, Ni-7, and Ni–15 at.% W alloys. In the diffraction profile obtained from electrodeposited pure Ni, it is apparent that Ni (111) is the most closely packed crystal plane, and appears as a main peak. In addition, its diffraction peaks shifted to a lower 2θ

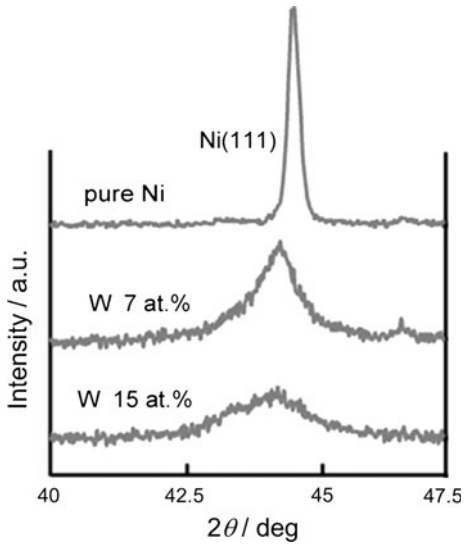

Fig. 2 X-ray diffraction profiles obtained from electrodeposited pure Ni, Ni–7, and 15 % W alloys

region as R_W^{depo} increased. This shift resulted from the formation of a solid solution phase (α phase) in the electrodeposited Ni–W alloys. On the contrary, the intensity of α (111) decreased, and the shape of its peaks broadened as R_W^{depo} increased, which indicates that the electrodeposited Ni–W alloys are composed of an ultrafine-crystalline phase. Weston et al. have also reported that an electrodeposited Co–W alloy consists of a nanocrystalline phase with R_W^{depo} that is higher than ca. 20 %. The nanocrystalline structure is formed by W atoms segregated from a supersaturated Co–W solid solution phase into grain boundaries at the W content range ($R_W^{depo} > 20$ %) [23]. However, in this study, the segregation of W atoms in the grain boundaries of electrodeposited Ni–15 at.% W alloys were not observed.

Figure 3 shows the relationship between R_W^{depo} and the crystal lattice constants of α phase (a_{Ni-W}). With an increase in R_W^{depo} up to ca. 15 %, a_{Ni-W} also increased

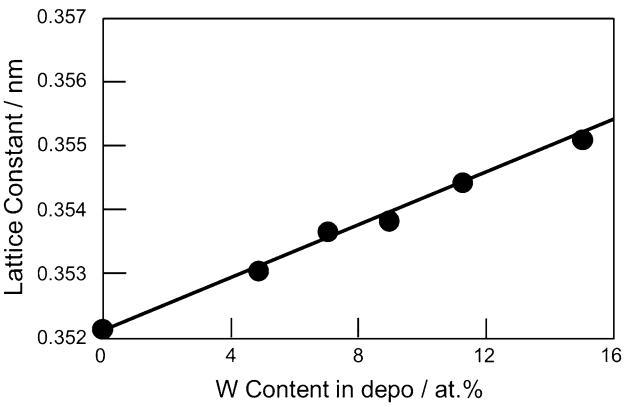

Fig. 3 Relationship between W content in Ni–W alloy deposits (R_W^{depo}) and the lattice constants (a_{Ni-W})

linearly. The lattice constants of fcc-Ni (a_{Ni}) and bcc-W (a_W) are 0.352 and 0.316 nm, respectively. Nevertheless, the atomic radii of Ni (r_{Ni}) and W (r_W) are 0.124 and 0.139 nm, respectively, so r_W is larger than r_{Ni}, and R_W^{depo} is less than ca. 15 %. Hence, a_{Ni-W} will increase with increasing R_W^{depo} when W atoms are substitutionally alloyed in a fcc-Ni matrix lattice. According to the phase diagram of a Ni–W binary alloy system [24], the solubility limit of W in α phase is ca. 12 at.%, and a Ni_4W intermetallic compound phase is formed at the composition of Ni–20 at.% W. Therefore, in this study, electrodeposited Ni–15 at.% W alloys are composed of a substitutional α′ phase.

Figure 4 shows SEM images of the electrodeposited Ni–15 % W alloy nanowire arrays that are separated from polycarbonate membrane filters and have pore diameters of 160 nm (a), (b) and 80 nm (c), (d). The diameters and lengths of the nanowires correspond well to those of the nanochannels. The cylindrical shape of these nanowires was also precisely transferred from that of the nanochannels, and the aspect ratio of the nanowires reached ca. 75. The length of the nanowires were allowed to range up to 6 μm by controlling the deposition time, while the diameter of the nanowires was fixed to around 80 or 160 nm. The array density (number of nanowires per substrate area) is ca. 6 μm^{-2}. The lateral areas of each nanowire are estimated at 1.4 and 2.8 μm^2. Hence, the surface area of each nanowire array is estimated at 10 and 18 times larger value than that of thin film. Kim et al. [25] have reported that a ferromagnetic Ni–Si alloy nanowire array with an extremely large specific surface area can be applied to a T cell separation device. The dimension of the Ni–Si alloy nanowire array developed by Kim et al. was similar to that of the Ni–W alloy nanowire array obtained in this study. Therefore, ferromagnetic Ni–W alloy nanowire arrays can also be applied to biological cell separation as well as magnetic field sensors. Figure 5 shows a TEM bright field image (a) and an electron diffraction pattern (b) of an electrodeposited Ni–15 % W alloy nanowire that is separated from a polycarbonate membrane filter. As shown in Fig. 5a, large crystal grains, each with a diameter that is more than several tens of nanometers, were not observed in

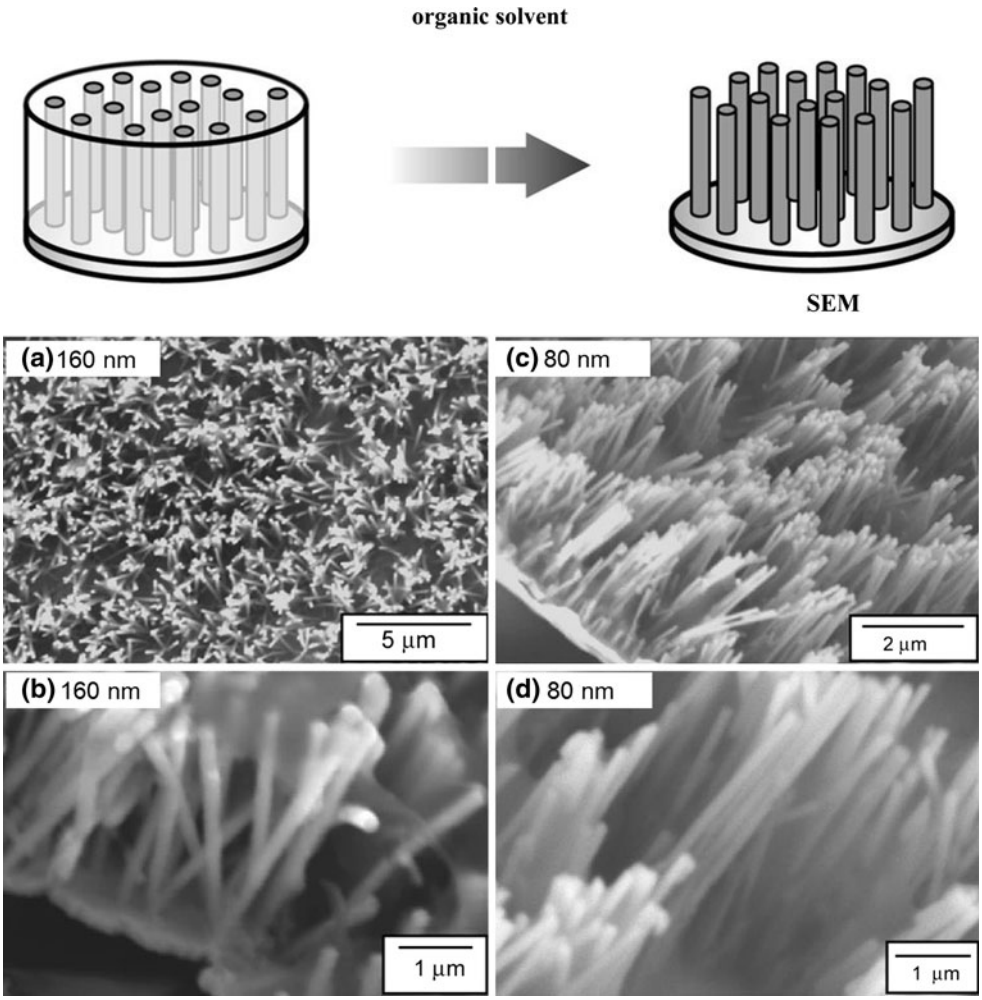

Fig. 4 SEM images of Ni–15 % W alloy nanowires electrodeposited into polycarbonate membrane filters with pore diameters of 160 nm (**a**, **b**) and 80 nm (**c**, **d**). Nanowires were separated from the polycarbonate membrane templates

the electrodeposited Ni–15 % W alloy nanowire. Furthermore, the electron diffraction pattern is composed of broad rings, as shown in Fig. 5b, so an electrodeposited Ni–15 % W alloy nanowire consists of a nanocrystalline phase.

3.2 Magnetic properties of electrodeposited Ni–W alloy nanowires

Figure 6 shows the magnetization curves of an electrodeposited pure Ni thin film with a thickness of 10 μm (a), a Ni–15 % W alloy thin film with a thickness of 3 μm (b), pure Ni nanowires with a length of 6 μm and a diameter of 80 nm (c), and Ni–15 % W alloy nanowires with a length of 6 μm and a diameter of 80 nm (d). A magnetic field was applied in-plane (the dashed lines) and in perpendicular (the solid lines) directions to the film plane. Here, the perpendicular direction to the nanowire array film plane corresponds to the parallel direction to the long axis of the nanowires. The pure Ni thin film is easily magnetized in the in-plane direction, and its magnetization reaches saturation at <1 kOe, as shown in Fig. 6a. The coercive force of this thin film is ca. 100 Oe. On the contrary, the pure Ni thin film hardly magnetized in the perpendicular direction due to the demagnetizing field caused by the inverse magnetic poles generated on the film's surface. The effective magnetic field, H_{eff}, can be expressed by the following equation:

$$H_{\text{eff}} = H_{\text{a}} - H_{\text{d}} = H_{\text{a}} - f_{\text{d}} \cdot M/\mu_0 \quad (1)$$

Here, H_{a}, H_{d}, f_{d}, M, and μ_0 are the applied magnetic field, demagnetizing field, factor of demagnetizing field, magnetic moment, and permeability constant, respectively. When the magnetic field is applied in a direction that is perpendicular to the film plane, f_{d} will be the maximum value. In this case, H_{d} also becomes the maximum value, so H_{eff} will be the minimum value and thus not enough to reach the saturation of magnetization. On the contrary, when the magnetic field is applied in the in-plane direction to the film plane, f_{d} will be almost zero. Therefore, H_{eff} will be equal to H_{a}. Zhou et al. [26] have also reported that the coercive force depends strongly on the film thickness in electrodeposited NiFeMo alloy thin films. Their experimental results also support H_{d} depends on f_{d} that is estimated from the aspect ratio of magnetized samples.

As shown in Fig. 6b, the magnetization of the Ni–15 % W alloy reaches saturation at ca. 2.5 kOe, even in the perpendicular direction. The magnetic moment, M, of the Ni–W alloys will decrease as the non-magnetic W decreases. As shown in equation (1), the demagnetizing field, H_{d}, is in proportion to the magnetic moment, M,

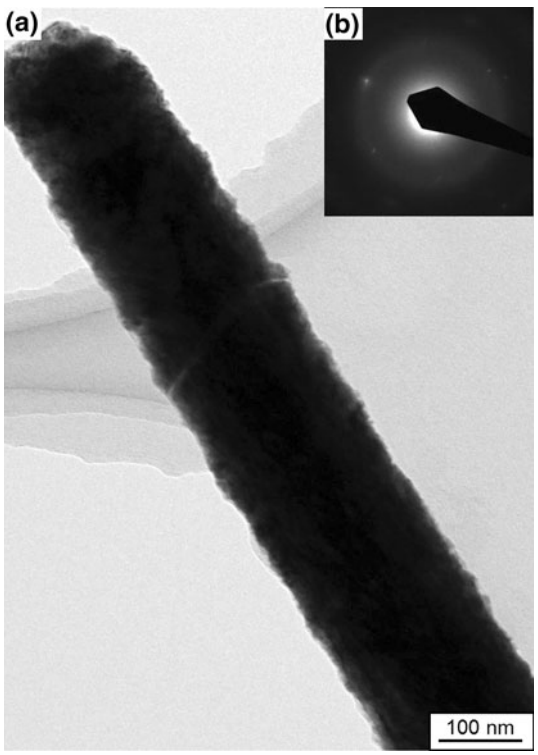

Fig. 5 TEM bright field image (**a**) and an electron diffraction pattern (**b**) of an electrodeposited Ni–15 % W alloy nanowire

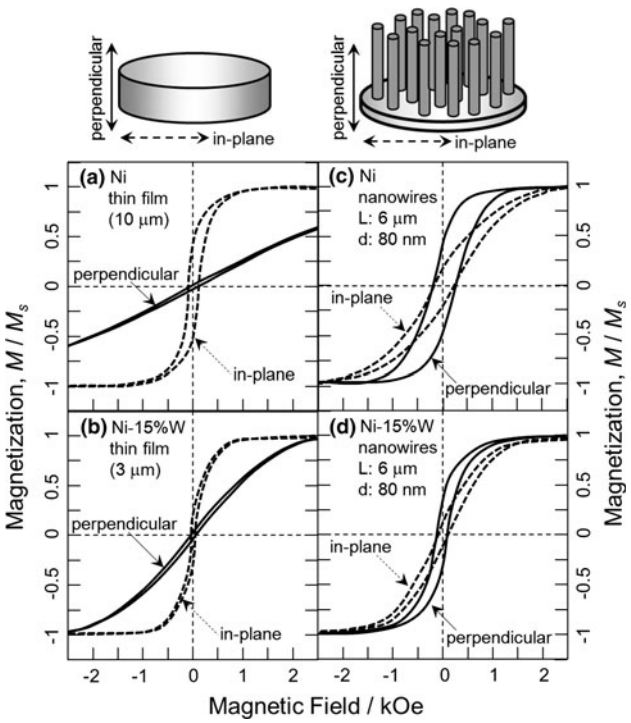

Fig. 6 Magnetization curves of an electrodeposited Ni thin film with a thickness of 10 mm (**a**), a Ni–15 % W alloy thin film with a thickness of 3 mm (**b**), Ni nanowires with lengths of 6 mm and diameters of 80 nm (**c**), and Ni–15 % W alloy nanowires with lengths of 6 mm and diameters of 80 nm (**d**). A magnetic field was applied in-plane (*dashed lines*) and perpendicular (*solid lines*) to the film's plane

which generates inverse magnetic poles on the surfaces that are perpendicular to the magnetic field. Sulitanu [27] has reported that Ni–W alloy thin films with perpendicular magnetic anisotropy can be obtained due to the binary phase structure with an isolated columnar nanocrystalline phase surrounded by an amorphous-like phase ($4\ \% < R_W^{depo} < 5\ \%$). The present report has also estimated that the perpendicular magnetic anisotropy in the alloy films arises from the magnetoelastic anisotropy associated with in-plane internal stress and positive magnetostriction. Hence, the magnetization behavior in the perpendicular direction observed in this study resulted from the small demagnetizing field (H_d) and the small K_c that is induced from a nanocrystalline phase in the alloy films. On the other hand, as shown in Fig. 6c, d, pure Ni and Ni–15 at.% W alloy nanowire arrays are easily magnetized even in a perpendicular direction because of the extremely small H_d that arises from the low density of the inverse magnetic poles generated on the edges of nanowires.

The coercive force (H_c) of pure Ni and Ni–15 % W alloy thin films are ca. 100 and 20 Oe, respectively, as shown in Fig. 6a, b. On the other hand, as shown in Fig. 6c, d, the H_c of pure Ni and Ni–15 % W alloy nanowire arrays are ca. 200 and 80 Oe, respectively. Fig. 7 illustrates the relationship between R_W^{depo} and H_c. With an increase in R_W^{depo}, H_c decreases, and the soft magnetic properties of the Ni–15 % W alloy thin films and nanowire arrays improve. As shown in Fig. 2 and 5, the crystal grain size of the electrodeposited Ni–W alloys decreases with an increase in R_W^{depo}. Herzer et al. [28] have reported that the H_c of ferromagnetic nanocrystalline alloys decreases with the decreasing average crystal grain size (D) in the range of less than ca. 50 nm, as shown in the following equation:

$$H_c = fD^6 \quad (2)$$

Here, f is a proportional constant. According to equation (2), H_c decreases as D decreases, so the H_c of electrodeposited Ni–W alloys also decreases with an increase in R_W^{depo} due to the decrease in D that the latter change causes. Consequently, the isotropic magnetization behavior of electrodeposited Ni–15 % W alloy nanowire arrays results from increasing H_{eff} due to decreasing f_d in the perpendicular direction to the array film plane and from decreasing H_c due to decreasing D.

Electrodeposited Ni–15 % W alloy is composed of a substitutional supersaturated solid solution phase (α' phase), as shown in Fig. 2 and 3. Hence, a certain residual strain seems to exist in an as-deposited alloy. It has been reported that the H_c of Ni alloys increases as the residual strain increases [29]. Therefore, it is predicted that the H_c of electrodeposited Ni–15 % W alloys with a supersaturated solid solution phase (α' phase) will decrease as the residual strain decreases via a thermal annealing treatment.

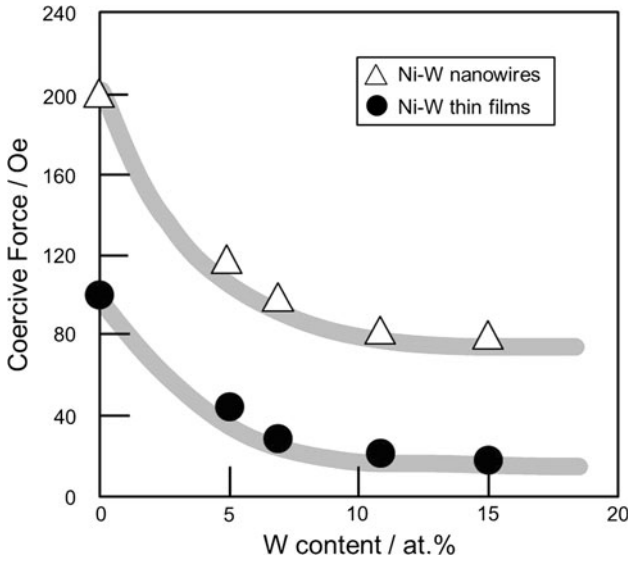

Fig. 7 Effects of W content (R_W^{depo}) in Ni–W alloy thin films and nanowires on coercive force

4 Conclusions

R_W^{depo} increased with an increase in R_W^{bath}, and R_W^{depo} was diluted ca. 0.4 times lower than R_W^{bath}. It is estimated that the dilution of W atoms in the alloy deposits, which occurs when the alloy is placed into a solution containing Ni^{2+} ions, will be caused by the small reduction ability of electrodeposited Ni. Electrodeposited Ni–15 % W alloys consist of a supersaturated solid solution phase with a nanocrystalline structure. Pure Ni thin film is hardly magnetized in the perpendicular direction, whereas the magnetization of the Ni–15 % W alloy thin film reaches saturation at ca. 2.5 kOe, even in a perpendicular direction, because H_d decreases with decreasing M. The H_c of electrodeposited Ni–W alloy thin films decreases to ca. 20 Oe with an increase in R_W^{depo} to around 15 %. On the other hand, the Ni–15 % W alloy nanowire array is isotropically magnetized in both directions, and the H_c of the alloy nanowire array is ca. 80 Oe, which is smaller than that of a pure Ni nanowire array. The alloy's coercive force is smaller, because the H_d decreased in response to reductions in f_d and M. Therefore, this study has demonstrated that the electrodeposited Ni–W alloy nanowire arrays can be applied to a nanoscale magnetic field sensor and exhibit isotropic magnetization responses, and the soft magnetic property can be improved by increasing R_W^{depo} up to ca. 15 %.

Acknowledgments This study was supported in part by TDK Corporation, Mitutoyo Association for Science & Technology, Yazaki Memorial Foundation for Science & Technology, Research Foundation for Materials Science, Japan Society for the Promotion of Science (Grant-in-aid for Scientific Research C : No. 19560734).

References

1. Yamasaki T (2001) High-strength nanocrystalline Ni-W alloys produced by electrodeposition and their embrittlement behaviors during grain growth. Scripta Mater 44:1497-1502
2. Donten M, Cesiulis H, Stojek Z (2000) Electrodeposition and properties of Ni-W, Fe-W and Fe-Ni-W amorphous alloys. Electrochim Acta 45:3389-3396
3. Ahmad J, Asami K, Takeuchi A, Louzguine DV, Inoue A (2003) High strength Ni-Fe-W and Ni-Fe-W-P alloys produced by electrodeposition. Mater Trans 44:1942-1947
4. Brenner A (1963) Electrodeposition of alloys. Academic Press, New York
5. Panagopoulos CN, Papachristos VD, Wahlstrom U, Leisner P, Christoffersen LW (2000) Ni-P-W multilayered alloy coatings produced by pulse plating. Scripta Mater 43:677-683
6. Schuh CA, Nieh TG, Iwasaki H (2003) The effect of solid solution W additions on the mechanical properties of nanocrystalline Ni. Acta Mater 51:431-443
7. Xu L, Du J, Ge S, He N, Li S (2009) Preparation and characterization of nanocrystalline Fe–Ni–Cr alloy electrodeposits on Fe substrate. J Appl Electrochem 39:713-717
8. Chassaing E, Portail N, Levy AF, Wang G (2004) Characterisation of electrodeposited nanocrystalline Ni–Mo alloys. J Appl Electrochem 34:1085-1091
9. Cornelius TW, Toimil-Molares ME, Neumann R, Karim S (2006) Finite-size effects in the electrical transport properties of single bismuth nanowires. J Appl Phys 100:114307
10. Ohgai T, Tanaka Y, Fujimaru T (2012) Soft Magnetic Properties of Ni-Cr and Co-Cr Alloy Thin Films Electrodeposited from Aqueous Solutions Containing Trivalent Chromium Ions and Glycine. J Appl Electrochem 42:893–899
11. Ohgai T, Tanaka Y, Washio R (2013) Nanocrystalline Structure and Soft Magnetic Properties of Nickel-molybdenum Alloy Thin Films Electrodeposited from Acidic and Alkaline Aqueous Solutions. J Solid State Electrochem 17:743-750
12. Sulitanu N (2002) Electrochemical deposition of novel nanostructured magnetic thin films for advanced applications. Mater Sci Eng B 95:230-235
13. Bas JA, Calero JA, Dougan MJ (2003) Sintered soft magnetic materials: Properties and applications. J Magn Magn Mater 254-255:391
14. Pommier J, Meyer P, Penissard G, Ferre J, Bruno P, Renard D (1990) Magnetization Reversal in Ultrathin Ferromagnetic Films with Perpendicular Anisotropy: Domain Observations. Phys Rev Lett 65:2054-2057
15. Huang Q, Davis D, Podlaha EJ (2006) Electrodeposition of FeCoNiCu nanowires. J Appl Electrochem 36:871-882
16. Ohgai T, Enculescu I, Zet C, Westerberg L, Hjort K, Spohr R, Neumann R (2006) Magneto-sensitive nickel nanowires fabricated by electrodeposition into multi- and single-ion track templates. J Appl Electrochem 36:1157-1162
17. Ohgai T, Hjort K, Spohr R, Neumann R (2008) Electrodeposition of cobalt based ferro-magnetic metal nanowires in polycarbonate films with cylindrical nanochannels fabricated by heavy-ion-track etching. J Appl Electrochem 38:713-719
18. Spohr R, Zet C, Fischer BE, Kiesewetter H, Apel P, Gunko I, Ohgai T, Westerberg L (2010) Controlled fabrication of ion track nanowires and channels. Nucl Inst Meth Phys Res B 268:676-686
19. Ohgai T, Washio R, Tanaka Y (2012) Anisotropic magnetization behavior of electrodeposited nanocrystalline Ni-Mo alloy thin films and nanowires array. J Electrochem Soc 159:H800-H804
20. Metzler OY, Zhu L, Gileadi E (2003) The anomalous codeposition of tungsten in the presence of nickel. Electrochim Acta 48:2551-2562
21. Admon U, Daniel MP, Grunbaum E, Lodder JC (1987) Magnetic properties of electrodeposited Co-W thin films. J Appl Phys 62:1943-1947
22. Fukushima H, Akiyama T, Akagi S, Higashi K (1979) Role of iron-group metals in the induced codeposition of molybdenum from aqueous solution. Trans Jpn Inst Met 20:358-364
23. Weston DP, Harris SJ, Shipway PH, Weston NJ, Yap GN (2010) Establishing relationships between bath chemistry, electrodeposition and microstructure of Co–W alloy coatings produced from a gluconate bath. Electrochim Acta 55:5695–5708
24. Hansen M, Anderko K (1958) Constitution of binary alloys. McGraw-Hill, New York
25. Kim DJ, Seol JK, Lee MR, Hyung JH, Kim GS, Ohgai T, Lee SK (2012) Ferromagnetic nickel silicide nanowires for isolating primary $CD4^+$ T lymphocytes. Appl Phys Lett 100:163703
26. Zhou Q, Heard PJ, Schwarzacher W (2011) Fabrication and magnetic properties of patterned NiFeMo films electrodeposited in self-assembled nanosphere templates. J Appl Phys 109:054313
27. Sulitanu N (2001) Structural origin of perpendicular magnetic anisotropy in Ni-W thin films. J Magn Magn Mater 231:85-93
28. Hernando A, Marin P, Vazquez M, Barandiaran JM, Herzer G (1998) Thermal dependence of coercivity in soft magnetic nanocrystals. Phys Rev B 58:366-370
29. Szabó S, Kis-Varga M, Beke DL, Juhász R (2000) Effect of residual strain, grain size and Fe impurities on magnetic properties of nanocrystalline Ni(Fe) alloys. J Magn Magn Mater 215–216:60-62